Rock and Soil Mechanics

Volume 43 | Issue 8 Article 4

10-9-2022

Elastic-plastic deformation of surrounding rocks under graded yielding support of tunnel

Jian-hua DONG
Western Engineering Research Center of Disaster Mitigation in Civil Engineering of Ministry of Education, Lanzhou University of Technology, Lanzhou, Gansu 730050, China

Bin XU
Western Engineering Research Center of Disaster Mitigation in Civil Engineering of Ministry of Education, Lanzhou University of Technology, Lanzhou, Gansu 730050, China

Xiao-lei WU
Western Engineering Research Center of Disaster Mitigation in Civil Engineering of Ministry of Education, Lanzhou University of Technology, Lanzhou, Gansu 730050, China

Bo LIAN
Western Engineering Research Center of Disaster Mitigation in Civil Engineering of Ministry of Education, Lanzhou University of Technology, Lanzhou, Gansu 730050, China

Custom Citation

DONG Jian-hua, XU Bin, WU Xiao-lei, LIAN Bo, . Elastic-plastic deformation of surrounding rocks under graded yielding support of tunnel[J]. Rock and Soil Mechanics, 2022, 43(8): 2123-2135.

Rock and Soil Mechanics 2022 43(8): 2123−2135 ISSN 1000−7598
https: //doi.org/10.16285/j.rsm.2021.6457 rocksoilmech.researchcommons.org/journal

Elastic-plastic deformation of surrounding rocks under graded yielding support of tunnel

DONG Jian-hua[1, 2], XU Bin[1, 2], WU Xiao-lei[1, 2], LIAN Bo[1, 2]

1. Key Laboratory of Disaster Prevention and Mitigation in Civil Engineering of Gansu Province, Lanzhou University of Technology, Lanzhou, Gansu 730050, China;
2. Western Engineering Research Center of Disaster Mitigation in Civil Engineering of Ministry of Education, Lanzhou University of Technology, Lanzhou, Gansu 730050, China

Abstract: In order to solve the failure of support structure of tunnel in high stress soft rock, based on the principle of reasonably releasing the stress in surrounding rocks and reducing the stress of support structure, a hydraulic tunnel graded yielding support structure is proposed. Considering the spatial effect of the excavation surface and the strain softening condition of the surrounding rocks, by analyzing the attenuation law of the virtual supporting force, the static balance equation of stress in the surrounding rocks, the virtual support force and the support reaction force is established. The synergy between the supporting structure and the surrounding rocks at each stage is studied to generate the relationship between the displacement and stress of the surrounding rocks in the whole deformation process of the support structure. The supporting effect of the proposed graded yielding support structure is revealed. The results show that the stress of surrounding rocks is significantly released at the two yielding stages and the deformation characteristics of surrounding rocks are consistent with the yielding characteristics of structure. The simulation results show the consistent variation trend with that of the theoretical values, which verifies the rationality of the theoretical analysis. The proposed yielding support structure can effectively release the stress in the surrounding rocks and reduce the stress of the supporting structure. It can avoid the yield failure of the support structure, solving the support problem of the tunnel in the soft rock with high stress, which can provide theoretical support for the application and development of the support structure.

Keywords: tunnel engineering; stress relief; whole process analysis; virtual support force; strain softening

1 Introduction

With the gradual implementation of the national strategy for the development of the western regions in China, a large number of traffic engineering projects including highway tunnels and railway tunnels have been built in western regions. However, the western regions belong to mountainous areas, which are characterized by strong crustal activities and high stress, and large deformation of tunnels in soft rocks is easily caused in these regions, such as the large deformation of the Wuqiaoling Tunnel, Muzhailing Tunnel, and Partridge Mountain Tunnel[1−3]. In the case of the large deformation of tunnels, strong support measures to resist tunnel deformation will lead to yielding failure and lining cracking of the support structures, which will reduce construction efficiency and affect construction safety[4−6]. Therefore, reasonable support measures are required to control the large deformation of tunnels, which is of great significance for accelerating the construction of tunnel engineering.

Up to now, many scholars have put forward the concept of "yielding support"[7−9], that is, ensuring construction safety by releasing the stress in surrounding rocks and reducing surrounding rock pressure. Kovari et al.[10] applied the concept of the yielding support earlier by grooving on the joints of steel arch frames to suit the deformation of the structure. Based on the large deformation characteristics of soft rocks, He et al.[11] developed the anchor bolt with constant resistance and large deformation, which greatly guarantees the stability of the support structure and has been widely used in China. Qiu et al.[12] proposed the "rigid–flexible–rigid" support structure with limited resistance and energy releasing capability, and applied it in the deep buried tunnel in old loess. Wang et al.[13−14] proposed the instant–strong–yielding joint support measures to reasonably release the deformation energy of the surrounding rocks and to reduce the force on the support structure. The above studies show that the application of the yielding support measures in the engineering can better suit the deformation requirements of the surrounding rocks and ensure the stability of the support structure.

In order to further analyze the mechanical characteristics of the interaction between the yielding support structure and the surrounding rocks, Wen et al.[15] established the composite arch mechanical model of surrounding rock–joint support based on the combined arch theory and the interaction between the joint support structure of anchor, shotcrete, and steel frame and the surrounding rocks, and obtained the deformation characteristics of the surrounding rocks under the joint support condition. Based on the strain softening model, Cui[16] introduced the virtual support force to analyze the interaction between the surrounding rocks and the support structure, and revealed the influence of the excavation process on the stress release of the surrounding rocks. Based on the spatial effect of the excavation surface, Hou et al.[17−18]

Received: 30 August 2021 Revised: 22 March 2022
This work was supported by the National Natural Science Foundation of China (52178335), the Central Government Guides Local Science and Technology Development Fund Project (YDZX20216200001739), the Longyuan Youth Innovation and Entrepreneurship Talent (Team Project) (2020RCXM120), the Ten Science and Technology Innovation Projects in Lanzhou City (2020-2-11), the High Value Patent Cultivation and Transformation Project of Gansu Intellectual Property Office (20ZSCQ034), and the Gansu Basic Research Innovation Group Project (20JR10RA205).
First author: DONG Jian-hua, male, born in 1980, PhD, Professor, mainly engaged in teaching and research on static and dynamic analysis of tunnel and slope soil. E-mail: djhua512@163.com

established the coupling model of the surrounding rocks and the support structure and analyzed the influence of the support structure on the deformation of the surrounding rocks. Based on the strain softening and volume expansion characteristics of the surrounding rocks, Fu[19] proposed the mechanical model of the deformation of the surrounding rocks to reveal the influence of strain softening conditions on the distribution of the fractured zones in the surrounding rocks. Wang et al.[20] analyzed the synergy between the surrounding rocks and the double-layer lining, and studied the influence of the primary lining and the secondary lining on the deformation of the surrounding rocks based on the strain softening conditions, thus the evolution of the load sharing between the two layers of linings was studied. Based on the deformation characteristics of the existing yielding support structure, the above studies analyzed the stress release and deformation law of the surrounding rocks in the yielding process.

At present, the U-shaped steel yielding arch frame is widely utilized, but it has a limited yielding amount, so it is difficult for the U-shaped steel yielding arch frame to suit the large deformation characteristics of the surrounding rocks in the tunnel in the soft rock under high stress. Therefore, in view of the self-support capacity of the surrounding rocks and the shortcomings of the current U-shaped steel yielding arch frame, the development of a new type of yielding support structure that can increase the yielding amount and reduce the force on the structure has important engineering meaning. Because the deformation characteristics of the new type of yielding support structure are not clear, it is necessary to carry out the analysis of the interaction between the new support structure and the tunnel, in order to further clarify the control effects of the new structure on the deformation of the surrounding rocks. This paper proposes a graded yielding support structure with an increasing yielding amount for the tunnel, which can improve the stress release rate of the surrounding rocks, reduce the force on the support structure, and ensure the stability of the surrounding rocks through two-stage shrinkage deformation. Based on the spatial effect of the excavation surface and the strain softening conditions of the surrounding rocks, the virtual support force is introduced to establish the calculation model of the multi-stage interaction between the new support structure and the tunnel, and the deformation characteristics of the surrounding rocks under the condition of yielding support are revealed by solving the calculation model, which provides a theoretical design basis for the later application of the yielding support structure in the tunnel in the soft rock under high stress.

2 Graded yielding support structure

2.1 Structural configuration

At present, the clamp is adopted as the yielding control component of the U-shaped steel yielding arch frame, and it fixes the overlap section of the U-shaped steel. When the friction between the section steel as well as the friction between the section steel and the clamp exceed the restraining force of the clamp, the slip is generated and the yielding function comes into play. The restraining force of the clamp continues to increase with the deformation of the steel frame at both ends, so the yielding point of the clamp is constantly changing. As the yielding amount increases, the deformation of the section steel leads to the shear of the clamp, causing damage to the clamp. In the case of ensuring the safety of the structure, the yielding amount of the U-shaped steel arch frame is generally small. In view of the shortcomings of the existing U-shaped steel yielding arch frame, this paper uses the hydraulic device as the yielding control component, and develops a new graded yielding support structure for the tunnel with a constant yielding point and a controllable yielding amount by means of a two-level yielding structure composed of radial and circumferential yielding structures. The radial yielding structure is composed of the outer arch frame and the hydraulic device, and the circumferential yielding structure is composed of the inner arch frame and the yielding anchor bolt.

During the construction process, the outer arch frame of the radial yielding structure is close to the surrounding rocks, and the inner arch frame of the circumferential yielding structure is located at the inner side of the outer arch. The outer and inner arch frames are connected by hydraulic devices. One end of the hydraulic device is connected to the outer arch frame, and the other end is connected to the inner arch frame through the pad. The yielding anchor bolt passes through the inner arch and the outer arch in location order. The anchorage section of the bolt is anchored in the deep stable rock layer, and the free end of the bolt is anchored at the inner side of the inner arch frame through the anchorage device and the bearing plate. The schematic diagram of the graded yielding support structure for the tunnel is shown in Fig. 1. Figure 1(a) depicts the locations of the radial yielding structure, the circumferential yielding structure, and the yielding anchor bolt. The radial yielding structure is located between the surrounding rocks and the circumferential yielding structure, and both the radial and circumferential yielding structures are suspended in the deep stable rock layer by the yielding anchor bolt. Figure 1(b) refines the position distribution of the radial yielding structure and the circumferential yielding structure. The radial yielding structure is deformed by the extrusion of the outer arch on the hydraulic device, and the circumferential yielding structure is deformed by the extrusion on the hydraulic device from the shrinkage deformation of the inner arch frames at both sides. Figure 1(c) shows the schematic diagram of the outer arch frame. The yielding deformation of the radial yielding structure is realized through the rotational deformation between the structures.

2.2 Deformation stages

The deformation of the graded yielding support structure for the tunnel is related to not only the elastic stiffness of the structure itself but also the distributions of the yielding point and the yielding amount of the structure. In order to analyze the deformation characteristics of the structure and the synergy between the structure and the surrounding rocks, the deformation of the structure is divided into the following five stages based on the yielding point and the multi-yielding characteristics.

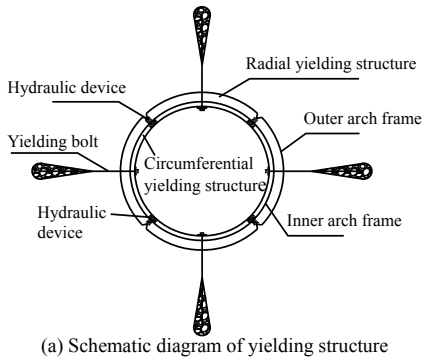

(a) Schematic diagram of yielding structure

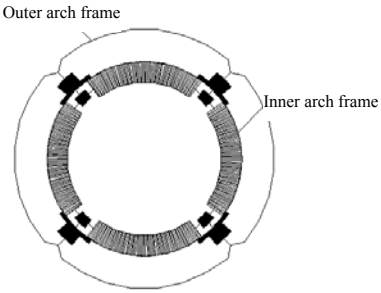

(b) Schematic diagram of radial and circumferential yielding structures

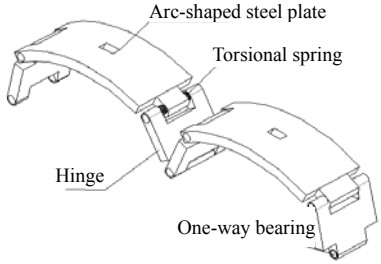

(c) Schematic diagram of outer arch frame

Fig. 1 Schematic diagram of tunnel graded yielding support structure

(1) The first strong support stage. At this stage, the internal force of the structure is less than the stress at the yielding point, and only elastic deformation occurs in the structure.

(2) Radial yielding stage. When the internal force of the radial yielding structure is greater than the stress at the yielding point of the structure, the outer arch shrinks and is deformed, the structure is in the yielding state with constant resistance, and the elastic deformation does not occur in the structure itself.

(3) Secondary strong support stage. After the radial yielding deformation is completed, the internal force of the circumferential yielding structure is less than the stress at the yielding point, and only the elastic deformation occurs in the structure under the action of the external force.

(4) Circumferential yielding stage. As the internal force of the circumferential yielding structure increases, the yielding deformation occurs after the yielding point is reached, and the internal force of the structure does not change.

(5) Subsequent strong support stage. After all the yielding is completed, only the elastic deformation occurs in the support structure until the support reaction force is equal to the stress of the surrounding rocks, and the structure remains stable.

2.3 Technical advantages

The yielding support structure has the following technical advantages over the existing steel frames:

(1) The anchor bolt, the outer arch frame, and the inner arch frame are all yielding support structures, which control the stability of the structure through the synergetic deformation in two aspects. On the one hand, the synergetic deformation between the outer arch frame and the surrounding rocks controls the stress release rate of the surrounding rocks. On the other hand, the shear effect between the structures is avoided through the synergetic deformation between the inner arch frame and the anchor bolt.

(2) The graded real-time yielding is controllable. The relief valve is adopted as the control element of the structure, and the threshold of the relief valve can control the yielding point of the structure according to the surrounding rock conditions, which can not only ensure construction safety but also reasonably release the stress in the surrounding rocks.

(3) The yielding ability of the structure is increased. Conventional yielding steel frames yields due to the stress concentration resulting from structural curvature changes, causing the weak yielding effect of the conventional structure. The curvature change of the new structure is reduced and the stress concentration of the structure is avoided through two yielding stages.

3 Principle of virtual support force

After the tunnel support is completed, the surrounding rocks and the support structure are synergistically deformed. In order to study the changes in the whole deformation process of the surrounding rocks, it is necessary to maintain a static equilibrium state at all the deformation stages. Therefore, additional forces are introduced to maintain the stability of the surrounding rocks at all the deformation stages.

Tunnel excavation belongs to a three-dimensional spatial problem. The spatial effect of tunnels is mainly concentrated in two aspects, including the circumferential stress effect in the cross-section and the "semi-circular dome" effect in the longitudinal section. Under the combined action of the longitudinal and transverse effects, the stress and displacement of the surrounding rocks change with the advance of the excavation surface. The "semi-circular dome" effect is manifested as the semi-circular dome deformation of the longitudinal tunnel wall and is mainly affected by the lithology of the surrounding rocks, the stress state, and the excavation surface. The spatial effect of the excavation surface described in this paper mainly refers to the "semi-circular dome" effect of the longitudinal section, that is, the effect of the excavation surface on the studied section[18]. The semi-circular dome effect in the longitudinal section is shown in Fig. 2.

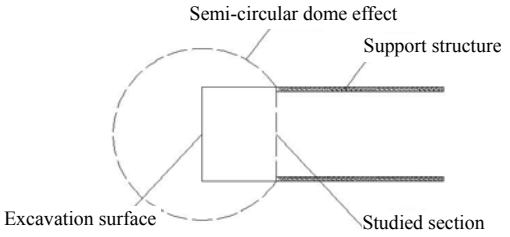

Fig. 2 Semi-circular dome effect

In order to represent the effect of the spatial effect of the excavation surface, a virtual support force is introduced, which converts the spatial effect into the radial force in the cross-section. The virtual support force is a quantitative analysis of the spatial effects of the excavation surface[16], and its physical meaning is to remove a section in the tunnel that is slowly deformed under the influence of the surrounding radial forces, which is called the virtual support force[21]. After the tunnel is excavated, the surrounding rocks remain stable under the action of the stress and virtual support force, as shown in Fig. 3. p_∞ is the in-situ stress; r_0 is the excavation radius of the tunnel; and p^* is the virtual support force.

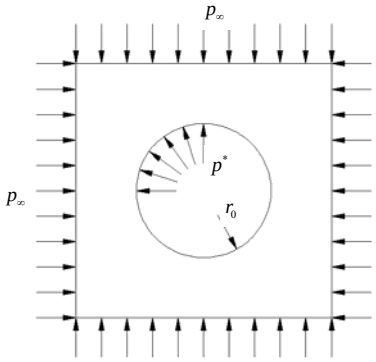

Fig. 3 Tunnel excavation model

As the excavation surface advances, the virtual support force gradually decreases until it disappears[21]. The change of the virtual support force with the advance of the excavation surface is shown in Fig. 4. $u_{r_0}^{p^*}$ is the displacement of the surrounding rocks; $u_{r_0}(\infty)$ is the maximum displacement of the surrounding rocks; and x is the distance from the excavation surface to the studied section.

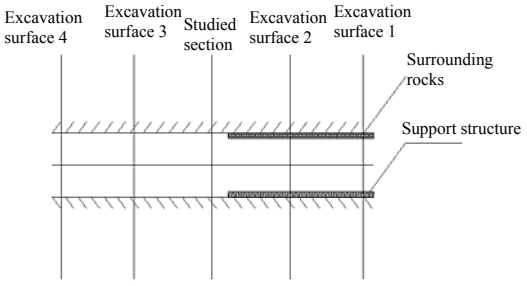

(a) Schematic diagram of virtual support force variation

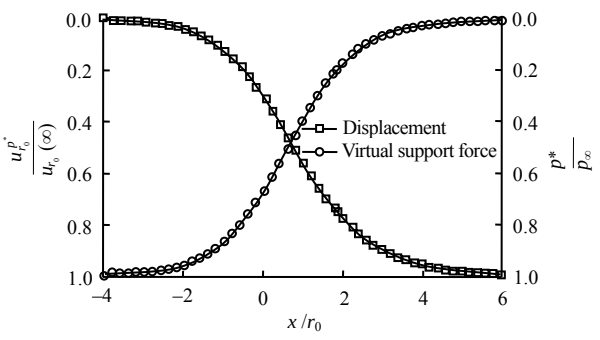

(b) Release curve of the virtual support force

Fig. 4 The change of virtual support force with the advance of the excavation surface

Figure 4(a) shows the relationship between the tunnel excavation surface and the studied section, and Fig. 4(b) shows the release law of the virtual support force. Figures 4(a) and 4(b) are combined to analyze the change law of the virtual support force:

(1) When the excavation reaches the excavation surface 1, the excavation surface is far from the studied section, whose surrounding rocks approximately maintain the in-situ stress state, and the release rate of the virtual support force is 0.

(2) When the excavation reaches the excavation surface 2, the excavation surface is closer to the studied section. The virtual support force in the studied section is released, and the surrounding rocks remain stable under the action of the virtual support force.

(3) When the excavation reaches the excavation surface 3, the studied section is located behind the excavation surface and the distance is relatively small. At this time, the stress of the surrounding rocks in the studied section is shared by the support structure and the virtual support force.

(4) When the excavation reaches the excavation surface 4, the excavation surface is far from the studied section, and the excavation disturbance on the studied section is approximately ignored. The stress of the surrounding rocks in the studied section acts on the support structure, and the virtual support force disappears.

The virtual support force can be obtained through experiments or simulations. Based on the maximum radius of the plastic zone of the surrounding rocks, Vlachopoulos et al.[22] obtained the expression of the virtual support force under ideal conditions. Alejano et al.[23] derived the relevant calculation method through the numerical simulation analysis. Literature [24–25] obtained the distribution of virtual support forces through field measurements and numerical simulations, and the distribution can be expressed as

$$\left.\begin{aligned} p^*(x) &= p_\infty\left(1-\delta_0^*\right)\exp(x*) \qquad (x*<0)\\ p^*(x) &= p_\infty\left(1-\delta_0^*\right)\exp\left(-\frac{3x*}{2r*}\right) \quad (x*\geqslant 0)\\ \delta_0^* &= \frac{1}{3}\exp\left(-0.15r^*\right) \end{aligned}\right\} \tag{1}$$

where $x* = \dfrac{x}{r_0}$; $r^* = \dfrac{r_{\max}}{r_0}$; $r_{\max}$ is the maximum plastic zone radius of the surrounding rocks without support; r_0 is the excavation radius of the tunnel; and x is the distance from the excavation surface to the studied section. $x>0$ means that the studied section is located behind the excavation surface, and $x<0$ indicates that the studied section is located in front of the excavation surface.

4 Deformation analysis of surrounding rocks based on strain softening

Based on strain softening conditions, the surrounding rocks are divided into the elastic zone, the softening zone, and the fractured zone according to the literature [26]. The new Austrian tunnelling method focuses on the self-bearing capacity of the surrounding rocks.

When the surrounding rocks are broken and lose the self-bearing capacity, the critical deformation when the fractured zone of the surrounding rocks appears is regarded as the maximum deformation allowed by the new Austrian tunnelling method construction, and the deformation can also be regarded as the limit yielding amount allowed by the yielding support measures. The calculation diagram for different surrounding rock zones is shown in Fig. 5.

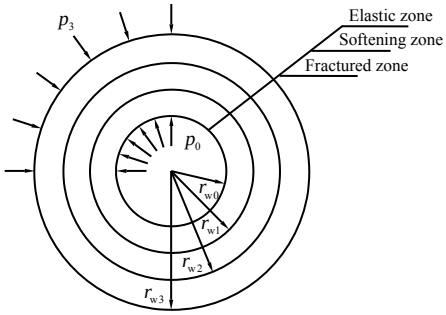

Note: p_0 is the inner boundary force; p_3 is the outer boundary force; r_{w0} is the radius of the inner boundary; r_{w1} is the radius of the fractured zone; r_{w2} is the radius of the softening zone; and r_{w3} is the radius of the elastic zone.

Fig. 5 Calculation diagram for different surrounding rock zones

4.1 Elastic zone

The general solution of the radial stress and tangential stress in the elastic zone can be obtained from the elastoplastic theory[23]:

$$\left.\begin{aligned}\sigma_r^{\mathrm{e}} &= \left(1-\frac{r_{\mathrm{w}2}^2}{r^2}\right)p_3+\frac{r_{\mathrm{w}2}^2}{r^2}p_2\\ \sigma_\theta^{\mathrm{e}} &= \left(1+\frac{r_{\mathrm{w}2}^2}{r^2}\right)p_3-\frac{r_{\mathrm{w}2}^2}{r^2}p_2\end{aligned}\right\} \tag{2}$$

where p_2 is the radial stress at the boundary between the elastic zone and the plastic zone and r is the distance between the calculated location and the center of the tunnel.

The radial elastic displacement at this location can be expressed as

$$u_r^{\mathrm{e}}=\frac{(1+\nu)r_{\mathrm{w}2}^2}{E_{\mathrm{w}}r}(p_3-p_2) \tag{3}$$

where E_{w} is the elastic modulus of the surrounding rocks and ν is the Poisson's ratio of the surrounding rocks.

4.2 Softening zone

The stress distribution of the softening zone can be expressed based on the inner and outer boundary forces. p_1 represents the radial stress at the inner boundary of the softening zone, and the stress distribution can be expressed as

$$\left.\begin{aligned}\sigma_r^{\mathrm{e}} &= \left(1-\frac{r_{\mathrm{w}1}^2}{r^2}\right)p_2+\frac{r_{\mathrm{w}1}^2}{r^2}p_1\\ \sigma_\theta^{\mathrm{e}} &= \left(1+\frac{r_{\mathrm{w}1}^2}{r^2}\right)p_2-\frac{r_{\mathrm{w}1}^2}{r^2}p_1\end{aligned}\right\} \tag{4}$$

Based on the M-C strength criterion, the relationship between the radial stress σ_r^{p} and the tangential stress $\sigma_\theta^{\mathrm{p}}$ in the softening zone is[26]

$$\sigma_\theta^{\mathrm{p}}=k\sigma_r^{\mathrm{p}}+\sigma_{\mathrm{c}}^{\mathrm{p}} \tag{5}$$

where $k=\dfrac{1+\sin\varphi}{1-\sin\varphi}$; φ is the internal friction angle of the surrounding rocks; $\sigma_{\mathrm{c}}^{\mathrm{p}}$ is the post-peak strength of the rock, and $\sigma_{\mathrm{c}}^{\mathrm{p}}=\sigma_{\mathrm{c}}-M\left[\varepsilon_\theta^{\mathrm{p}}-\left(\varepsilon_\theta^{\mathrm{e}}\right)_{r=r_{\mathrm{w}2}}\right]$, in which σ_{c} is the uniaxial compressive strength of the rock, M is the strain softening modulus, $\varepsilon_\theta^{\mathrm{p}}$ is the circumferential strain of the softening zone, and $\left(\varepsilon_\theta^{\mathrm{e}}\right)_{r=r_{\mathrm{w}2}}$ is the circumferential strain at the elastic boundary. According to $\sigma_{\mathrm{c}}^{\mathrm{p}}=\dfrac{2c'\cos\varphi}{1-\sin\varphi}$, $c'=\dfrac{1-\sin\varphi}{2\cos\varphi}$. $\sigma_{\mathrm{c}}^{\mathrm{p}}$ can be obtained.

The radial and circumferential stresses in the softening zone can be solved by uniting Eqs. (4) and (5):

$$\left.\begin{aligned}\sigma_r^{\mathrm{p}} &= (p_1+c'\cot\varphi)\left(\frac{r}{r_{\mathrm{w}1}}\right)^{\frac{2\sin\varphi}{1-\sin\varphi}}-c'\cot\varphi\\ \sigma_\theta^{\mathrm{p}} &= \frac{1+\sin\varphi}{1-\sin\varphi}(p_1+c'\cot\varphi)\left(\frac{r}{r_{\mathrm{w}1}}\right)^{\frac{2\sin\varphi}{1-\sin\varphi}}-c'\cot\varphi\end{aligned}\right\} \tag{6}$$

The displacement in the softening zone is related to the inner and outer boundary stresses and the softening characteristics of the rock mass. The general solution form u_r^{p} is consistent with the displacement in the elastic zone, so it can be expressed as

$$u_r^{\mathrm{p}}=\frac{(1+\nu)r_{\mathrm{w}2}^2}{E_{\mathrm{w}}r}(p_3-p_1) \tag{7}$$

4.3 Radius of softening zone

Based on the stress compatibility conditions, the radius of the softening zone can be expressed as

$$r_{\mathrm{w}2}=\left[\frac{(p_3+c\cot\varphi)(1-\sin\varphi)}{p_1+c\cot\varphi}\right]^{\frac{1-\sin\varphi}{2\sin\varphi}}r_{\mathrm{w}1} \tag{8}$$

4.4 Boundary stress between elastic and plastic zones

The stress at the boundary between the elastic and plastic zones satisfies the M-C yield criterion, and the boundary stress can be expressed as

$$p_2=p_3-(p_3+c\cot\varphi)\sin\varphi \tag{9}$$

4.5 Yielding deformation of arch frame

From the literature [27], it can be seen that the elastic deformation will be produced in the yielding arch frame under the action of external forces, and the shrinkage deformation will be produced in the structure due to the yielding structure, so the deformation of the yielding arch frame u^{p} can be divided into the elastic deformation u_{t} and the yielding deformation u_{r}, that is

$$u^{\mathrm{p}} = u_{\mathrm{t}} + u_{\mathrm{r}} \tag{10}$$

Assuming that the deformation of the cross-section of the steel frame is consistent, the equivalent stiffness of the steel frame can be expressed as

$$k_{\mathrm{g}} = \frac{E_{\mathrm{g}} A_{\mathrm{g}}}{s\left(r_0 - h_{\mathrm{s}}/2\right)^2} \tag{11}$$

where E_{g} is the elastic modulus of the steel arch frame; A_{g} is the cross-section area of the steel arch frame; s is the longitudinal spacing of the steel arch frames; and h_{s} is the cross-section height of the steel arch frame.

Based on the equivalent stiffness of the steel frame, the elastic deformation generated by the action of external forces is

$$u_{\mathrm{t}} = p_0 / k_{\mathrm{g}} \tag{12}$$

In order to obtain the elastic deformation of the steel frame under the pressure, the stress at the boundary of the softening zone is obtained according to the softening modulus:

$$p_{\mathrm{l}} = \frac{\left(p_3 + c\cot\varphi\right)\left(1-\sin\varphi\right)}{\left[\dfrac{2E_{\mathrm{w}}\left(c-c'\right)\cos\varphi}{M\left(1+v\right)\left(p_3+c\cot\varphi\right)\sin\varphi\left(1-\sin\varphi\right)}+1\right]^{\frac{\sin\varphi}{1-\sin\varphi}} - c\cot\varphi} \tag{13}$$

In Eq. (13), the cohesion c' in the softening zone is a variable, which is related to the deformation characteristics of the rock mass in the softening zone. Equations (3), (8), and (9), and the softening modulus are united to obtain the cohesion distribution of the softening zone:

$$c' = c - \left[\frac{u^{\mathrm{p}}}{r_{\mathrm{w1}}} - \frac{\left(1+v\right)}{E_{\mathrm{w}}}\left(p_3 + c\cot\varphi\right)\sin\varphi\right]\frac{M\left(1-\sin\varphi\right)}{2\cos\varphi} \tag{14}$$

Equations (12)–(14) are united to obtain the elastic deformation of the steel frame under the pressure. Equations (12)–(14) are combined with Eq. (10), and the yielding deformation of the arch frame can be obtained as

$$u_{\mathrm{r}} = \frac{2\left(c-c'\right)r_{\mathrm{w0}}\cos\varphi}{M\left(1-\sin\varphi\right)} + \frac{\left(1+v\right)r_{\mathrm{w0}}}{E_{\mathrm{w}}}\cdot \left(p_3 + c\cot\varphi\right)\sin\varphi - \frac{p_0 s\left(r_{\mathrm{w0}} - h_{\mathrm{s}}/2\right)}{E_{\mathrm{g}}A_{\mathrm{g}}} \tag{15}$$

4.6 Limit yielding amount

The yielding amount of the arch frame can be determined by the maximum allowable deformation of the surrounding rocks. When the stress in the rock mass reaches the residual strength σ_{c}^*, the fractured zone occurs in the surrounding rocks, and at this time the radius of the softening zone is the same as the radius of the excavation boundary, that is, $r_{\mathrm{w1}} = r_{\mathrm{w0}}$. The maximum inner boundary force $p_{0\max}$ can be calculated based on the softening modulus and Eqs. (3) and (7):

$$p_{0\max} = \frac{\left(p_3 + c\cot\varphi\right)\left(1-\sin\varphi\right)}{\left[\dfrac{2E_{\mathrm{w}}\left(c-c^*\right)\cos\varphi}{M\left(1+v\right)\left(p_3+c\cot\varphi\right)\sin\varphi\left(1-\sin\varphi\right)}+1\right]^{\frac{\sin\varphi}{1-\sin\varphi}} - c\cot\varphi} \tag{16}$$

The boundary force p_0 in Eq. (15) is replaced with the maximum inner boundary force $p_{0\max}$ to obtain the maximum yielding amount $u_{r\max}$ of the yielding arch frame allowed by the surrounding rocks in the excavation section:

$$u_{r\max} = \frac{2\left(c-c^*\right)r_{\mathrm{w0}}\cos\varphi}{M\left(1-\sin\varphi\right)} + \frac{\left(1+v\right)r_{\mathrm{w0}}}{E_{\mathrm{w}}}\cdot \left(p_3 + c\cot\varphi\right)\sin\varphi - \frac{p_{0\max} s\left(r_{\mathrm{w0}} - h_{\mathrm{s}}/2\right)}{E_{\mathrm{g}}A_{\mathrm{g}}} \tag{17}$$

5 Whole deformation process of surrounding rocks under yielding support condition

Based on the deformation synergy between the surrounding rocks and the structure, the deformation process of the surrounding rocks is divided into multiple stages. Before the excavation surface reaches the studied section, the surrounding rocks are partially deformed under the spatial effect of the excavation surface, that is, $u_0 = u_{\mathrm{c0}}$. The radial displacement at the initial strong support stage is assumed as u_{c1}, the radial displacement at the radial yielding stage is u_{c2}, the radial displacement at the secondary strong support stage is u_{c3}, the radial displacement at the circumferential yielding stage is u_{c4}, and the radial displacement at the subsequent strong support stage is u_{c5}. The yielding point and the yielding amount of the structure need to be set in advance. Then the yielding point q_0 and the yielding deformation u_{c2} and u_{c4} are known values. The elastic deformation of the structure u_{c1}, u_{c3}, and u_{c5} can be obtained based on Eq. (12) expressing the structure stiffness. Therefore, the correspondence between the deformation of the structure and the surrounding rocks is shown in Table 1.

Table 1 Displacement of surrounding rocks at different stages

Stages	Accumulated radial shrinkage of the yielding arch frame	Accumulated radial shrinkage of the surrounding rocks
First strong support stage	u_{z1}	u_1
Radial yielding stage	u_{z2}	u_2
Secondary strong support stage	u_{z3}	u_3
Circumferential yielding stage	u_{z4}	u_4
Subsequent strong support stage	u_{z5}	u_5

Note: The deformation of the surrounding rocks is $u_i = \sum_{n=0}^{i} u_{cn}$ and the radial deformation of the yielding arch frame is $u_{zi} = \sum_{n=1}^{i} u_{cn}$.

5.1 Deformation of surrounding rocks at the initial strong support stage

Before the excavation surface reaches the studied

section, the surrounding rocks remain stable under the action of the virtual support force. The surrounding rock stress p_0' and the virtual support force p_0^* are in a state of dynamic equilibrium:

$$p_0' = p_0^* = p_0\left[1-\frac{1}{3}\exp\left(-0.15\frac{r_{\max}}{r_{w0}}\right)\right] \tag{18}$$

At this stage, the surrounding rocks are still in an elastic state, and the boundary force p_2 of the elastic zone in Eq. (3) is replaced by p_0' to obtain the initial displacement u_0 of the surrounding rocks before the excavation surface reaches the studied section:

$$u_0 = \frac{(1+\nu)r_{w0}}{E_w}(p_3 - p_0') \tag{19}$$

When the excavation surface reaches the studied section, it is assumed that the surrounding rocks have not been deformed during the period from the excavation to the immediate support after the excavation. At this stage, part of the stress in the surrounding rocks is released with the advance of the excavation, while the rest part of the stress in the surrounding rocks is shared by the support reaction force and the virtual support force. As the virtual support force p^* is released, the support reaction force q increases. Before the support reaction force reaches the yielding point of the yielding arch frame, only the elastic deformation of the yielding arch frame occurs. Assuming that only the elastic deformation occurs in the surrounding rocks at the initial strong support stage, it can be seen from the deformation compatibility conditions that the deformation of the surrounding rocks is consistent with that of the yielding arch frame. The displacement of the surrounding rocks in the elastic zone provided by Eq. (3) can lead to the boundary force in the surrounding rocks at this stage:

$$p^{(1)}{}_0 = p_3 - \frac{u_1 E_w}{(1+\nu)r_{w0}} \tag{20}$$

where $p^{(1)}{}_0$ is the inner boundary force at the first strong support stage and is the resultant force of the virtual support force and the support reaction force, that is, $p^{(1)}{}_0 = p_1^* + q_1$.

From Eq. (12), it can be seen that the support reaction force provided by the yielding arch frame at this stage is

$$q_1 = u_{c1}k_g \tag{21}$$

Thus, combining Eqs. (20) and (21) can lead to the virtual support force at this stage:

$$p_1^* = p_3 - \frac{u_1 E_w}{(1+\nu)r_{w0}} - u_{c1}k_g \tag{22}$$

The virtual support force is related to the distance between the excavation surface and the studied section. The position of the excavation surface x_1 at the end of this stage can be calculated by substituting Eq. (22) calculating the virtual support force into Eq. (1):

$$x_1 = -\frac{2r_{\max}}{3}\cdot\ln\left(\frac{p_1^*}{p_\infty(1-\delta^*)}\right) \tag{23}$$

5.2 Deformation of surrounding rocks at the radial yielding stage

With the advance of the excavation, the support reaction force continues to increase. When the internal force of the support structure reaches the yielding point, the support reaction force provided by the yielding arch frame no longer increases, and the yielding deformation is produced in the structure. The virtual support force continues to decrease with the advance of the excavation, and the stress in the surrounding rocks, the virtual support force, and the support reaction force are in dynamic equilibrium:

$$p_2^* + q_2 = p^{(2)}{}_0 \tag{24}$$

Assuming that the surrounding rocks transit from the elastic state to the plastic state at this stage, the support reaction force at this stage remains unchanged, and the deformation of the surrounding rocks under the elastic limit condition u_2^{e} can be obtained by substituting Eq. (9) into Eq. (3):

$$u_2^{\mathrm{e}} = \frac{(1+\nu)r_{w0}}{E_w}(p_0\sin\varphi + c\cos\varphi) \tag{25}$$

The virtual support force under the elastic limit condition $p_2^{\mathrm{e}*}$ can be obtained by substituting Eq. (25) into Eq. (22):

$$p_2^{\mathrm{e}*} = p_3 - \frac{u_2^e E_w}{(1+\nu)r_{w0}} - q_2 \tag{26}$$

By substituting Eq. (26) into Eq. (1), the excavation distance of the section when the surrounding rocks are in the elastic limit state x_2 can be obtained:

$$x_2 = -\frac{2r_{\max}}{3}\cdot\ln\left(\frac{p_2^{\mathrm{e}*}}{p_\infty(1-\delta^*)}\right) \tag{27}$$

After the deformation of the surrounding rocks exceeds the elastic limit, the softening zones occur in the surrounding rocks. From Eq. (14), it can be seen that the attenuation law of the cohesion of the surrounding rocks in this zone is

$$c_2' = c - \left[\frac{u_2^p}{r_{w0}} - \frac{(1+\nu)}{E_w}(p_3 + c\cot\varphi)\sin\varphi\right]\frac{M(1-\sin\varphi)}{2\cos\varphi} \tag{28}$$

The inner boundary force of the plastic softening zone at this stage can be obtained according to Eq. (13):

$$p^{(2)}{}_0 = \frac{(p_3 + c\cot\varphi)(1-\sin\varphi)}{\left[\dfrac{2E_w(c-c_2')\cos\varphi}{M(1+\nu)(p_3+c\cot\varphi)\sin\varphi(1-\sin\varphi)}+1\right]^{\frac{\sin\varphi}{1-\sin\varphi}}} - c\cot\varphi \tag{29}$$

Substituting the support reaction force q_2 and the cohesion after the softening c_2' into Eq. (6) results in the virtual support force p_2^* at this stage:

$$p_2^* = \frac{(p_3 + c\cot\varphi)(1-\sin\varphi)}{\left[\dfrac{2E_w(c-c_2')\cos\varphi}{M(1+\nu)(p_3+c\cot\varphi)\sin\varphi(1-\sin\varphi)}+1\right]^{\frac{\sin\varphi}{1-\sin\varphi}}} - c\cot\varphi - q_2 \tag{30}$$

In order to obtain the position of the excavation surface during the deformation process of this stage, the excavation distance of the radial yielding stage is obtained by substituting Eq. (30) into Eq. (1):

$$x_2 = -\frac{2r_{\max}}{3}\cdot\ln\left(\frac{p_2^*}{p_\infty\left(1-\delta^*\right)}\right) \tag{31}$$

5.3 Deformation of surrounding rocks at the secondary strong support stage

At this stage, the circumferential yielding deformation of the yielding arch frame does not occur, and there is only elastic deformation in the structure. The internal force of the support structure continues to increase. The elastic deformation of the support structure ($u_{c3}+u_{c1}$) can be substituted into Eq. (21) representing the support reaction force, and the support reaction force of the structure acting on the surrounding rocks at this stage is obtained as

$$q_3 = \left(u_{c3}+u_{c1}\right)k_g \tag{32}$$

The cohesion of the surrounding rocks decreases with the deformation at this stage. The cohesion c_3' of the surrounding rocks at this stage is obtained by substituting the displacement u_3 into Eq. (14):

$$c_3' = c-\left[\frac{u_3}{r_{w0}}-\frac{(1+\nu)}{E_w}\left(p_3+c\cot\varphi\right)\sin\varphi\right]\frac{M\left(1-\sin\varphi\right)}{2\cos\varphi} \tag{33}$$

The cohesion c' in Eq. (13) expressing the boundary force of the surrounding rocks is replaced by the cohesion c_3' in the softening zone, and the inner boundary force $p_0^{(3)}$ of the surrounding rocks at this stage can be obtained as

$$p_0^{(3)} = \frac{\left(p_3+c\cot\varphi\right)\left(1-\sin\varphi\right)}{\left[\dfrac{2E_w\left(c-c_3'\right)\cos\varphi}{M\left(1+\nu\right)\left(p_3+c\cdot\cot\varphi\right)\sin\varphi\left(1-\sin\varphi\right)}+1\right]^{\frac{\sin\varphi}{1-\sin\varphi}}}-c\cot\varphi \tag{34}$$

The virtual support force p_3^* at this stage can be obtained by Eqs. (32) and (34):

$$p_3^* = \frac{\left(p_3+c\cot\varphi\right)\left(1-\sin\varphi\right)}{\left[\dfrac{2E_w\left(c-c_3'\right)\cos\varphi}{M\left(1+\nu\right)\left(p_3+c\cot\varphi\right)\sin\varphi\left(1-\sin\varphi\right)}+1\right]^{\frac{\sin\varphi}{1-\sin\varphi}}}-c\cot\varphi-q_3 \tag{35}$$

The obtained virtual support force p_3^* is substituted into Eq. (1) to obtain the excavation distance x_3 at the secondary strong support stage:

$$x_3 = -\frac{2r_{\max}}{3}\cdot\ln\left(\frac{p_3^*}{p_\infty\left(1-\delta^*\right)}\right) \tag{36}$$

5.4 Deformation of the surrounding rocks at the circumferential yielding stage

When the internal force of the structure reaches the yielding point of the inner arch frame, the circumferential shrinkage deformation is produced in the inner arch frame. The surrounding rock stress, the virtual support force, and the support reaction force are in dynamic equilibrium during this stage. Same as the above analysis, replacing the u^p in Eq. (14) by the deformation of the surrounding rocks u_4 leads to the cohesion c_4' at this stage:

$$c_4' = c-\left[\frac{u_4}{r_{w0}}-\frac{(1+\nu)}{E_w}\left(p_3+c\cot\varphi\right)\sin\varphi\right]\frac{M\left(1-\sin\varphi\right)}{2\cos\varphi} \tag{37}$$

The cohesion c_3' in Eq. (35) is replaced by the cohesion c_4' of the softening zone to obtain the inner boundary force of the surrounding rocks $p_0^{(4)}$ at this stage:

$$p_0^{(4)} = \frac{\left(p_3+c\cot\varphi\right)\left(1-\sin\varphi\right)}{\left[\dfrac{2E_w\left(c-c_4'\right)\cos\varphi}{M\left(1+\nu\right)\left(p_3+c\cot\varphi\right)\sin\varphi\left(1-\sin\varphi\right)}+1\right]^{\frac{\sin\varphi}{1-\sin\varphi}}}-c\cot\varphi \tag{38}$$

The resultant force of the virtual support force p_4^* and the support reaction force q_4 is the inner boundary force $p_0^{(4)}$, and the virtual support force p_4^* at this stage is obtained by Eq. (38):

$$p_4^* = \frac{\left(p_3+c\cot\varphi\right)\left(1-\sin\varphi\right)}{\left[\dfrac{2E_w\left(c-c_4'\right)\cos\varphi}{M\left(1+\nu\right)\left(p_3+c\cot\varphi\right)\sin\varphi\left(1-\sin\varphi\right)}+1\right]^{\frac{\sin\varphi}{1-\sin\varphi}}}-c\cot\varphi-q_4 \tag{39}$$

The virtual support force p_4^* is substituted into Eq. (1) to obtain the excavation distance x_4 of the circumferential yielding stage:

$$x_4 = -\frac{2r_{\max}}{3}\cdot\ln\left(\frac{p_4^*}{p_\infty\left(1-\delta^*\right)}\right) \tag{40}$$

5.5 Deformation of surrounding rocks at the subsequent strong support stage

After the yielding deformation is completed, only the elastic deformation occurs in the structure. With the advance of the excavation section, the virtual support force gradually decreases, and the internal force of the structure continues to increase. The elastic deformation is substituted into Eq. (21) to obtain the support reaction force:

$$q_5 = \left(u_{c1}+u_{c3}+u_{c5}\right)k_g \tag{41}$$

The cohesion of the softening zone c_5' is obtained by substituting the deformation of surrounding rocks u_5 at this stage into Eq. (14):

$$c_5' = c-\left[\frac{u_5}{r_{w0}}-\frac{(1+\nu)}{E_w}\left(p_3+c\cot\varphi\right)\sin\varphi\right]\frac{M\left(1-\sin\varphi\right)}{2\cos\varphi} \tag{42}$$

Substituting the cohesion c_5' into Eq. (13) leads to the inner boundary force $p^{(5)}{}_0$ of the surrounding rocks:

$$p^{(5)}{}_0 = \frac{(p_3 + c\cot\varphi)(1-\sin\varphi)}{\left[\frac{2E_w(c-c_5')\cos\varphi}{M(1+v)(p_3+c\cot\varphi)\sin\varphi(1-\sin\varphi)}+1\right]^{\frac{\sin\varphi}{1-\sin\varphi}}} - c\cot\varphi \tag{43}$$

At this stage, the virtual support force p_5^* gradually decays, and the corresponding virtual support force can be obtained:

$$p_5^* = \frac{(p_3 + c\cot\varphi)(1-\sin\varphi)}{\left[\frac{2E_w(c-c_5')\cos\varphi}{M(1+v)(p_3+c\cot\varphi)\sin\varphi(1-\sin\varphi)}+1\right]^{\frac{\sin\varphi}{1-\sin\varphi}}} - c\cot\varphi - q_5 \tag{44}$$

Substituting the virtual support force p_5^* into Eq. (1) yields the excavation distance x_5 of this stage:

$$x_5 = -\frac{2r_{\max}}{3}\cdot\ln\left(\frac{p_5^*}{p_\infty(1-\delta^*)}\right) \tag{45}$$

6 Case studies

In order to further reveal the effect of the yielding support structure, the stress release and deformation law of the surrounding rocks under the yielding support are studied by case studies. The Shawan tunnel is located in a high-stress regime, and excessive convergence deformation occurs during the construction. The stratigraphic lithology is middle and lower Silurian grey-black slate interlayered with limestone and metasandstone. The rock mass is seriously weathered, and the surrounding rock grades are IV and V. The foliation develops in the slate, and there is a poor combination of foliation surfaces. The slate belongs to the relatively soft rock with significant crumpling deformation and uneven hardness, and its weathering resistance ability difference is significant. The collapse along the foliation surface or the block dropping is easy to occur for the slate. The maximum buried depth of the tunnel is 350 m. In order to verify the deformation control effect of the yielding support on the surrounding rocks, the deformation characteristics of the surrounding rocks are analyzed by setting the yielding amount of the outer arch frame as 0.15 m and that of the inner arch frame as 0.05 m. The mechanical parameters of the surrounding rocks and the support structure are shown in Table 2.

Table 2 Mechanical parameters of surrounding rocks and support structure

Structure	Elastic modulus /GPa	Poisson's ratio	Internal friction angle/(°)	Cohesion /MPa	Softening modulus /MPa
Surrounding rocks	0.8	0.35	30	1.5	1
Support structure	200	0.25			

Figure 6 shows the variation of these three types of stresses (stress in the surrounding rocks, virtual support force, and support reaction force) with the deformation of the surrounding rocks. It can be seen from the deformation stages of the surrounding rocks that the stress release of the surrounding rocks slows down after the elastic–plastic junction. It can be seen from the deformation stages of the support structure that the virtual support force is reduced before the support structure is applied, resulting in the release of the stress in the surrounding rocks. After the support structure is applied, the stress release of the surrounding rocks is still characterized by the reduction of the virtual support force at the yielding stage, while the stress release of the surrounding rocks is accompanied by a rapid increase in the support reaction force at the non-yielding stage. The results show that the support reaction force changes at multiple stages, which is in line with the theoretical curve of the yielding support. When the deformation of the surrounding rocks reaches 0.5 m, the spatial effect of the excavation surface no longer affects the deformation of the surrounding rocks, and the support structure maintains the stability of the surrounding rocks.

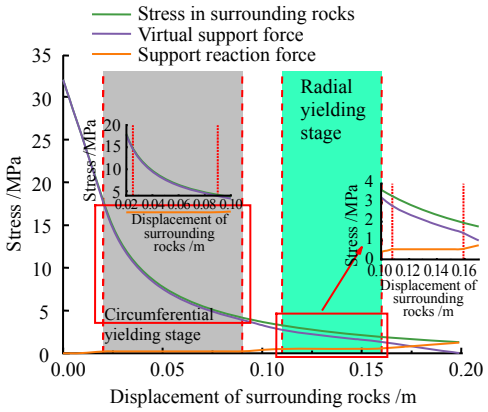

Fig. 6 Variation of stress with displacement

Figure 7 shows the relationship between these three types of stresses and the excavation distance. The release law of the virtual support force shown in Eq. (1) is only related to the distance from the excavation surface to the studied section. At the beginning of the excavation, the virtual support force is significantly reduced, and it is gradually released as the distance from the excavation surface to the studied section increases. At the early stages of the support, the significant release of the virtual support forces leads to the support reaction forces reaching the yielding point with a rapid increase. The support reaction force remains constant during the yielding stage and is balanced with the stress in surrounding rocks during the late support period. The stress release of the surrounding rocks is significant at the early stage of the excavation and the two yielding stages. The surrounding rocks are still in the elastic state at the early stage of the radial yielding stage, and their stress release is more significant.

7.1 Implementation of virtual support force

In the numerical simulation, the virtual support force is released by setting the amplitude curve in Abaqus. The release rate of the virtual support force

k^* is used as the control index of the amplitude curve, and it can be expressed as

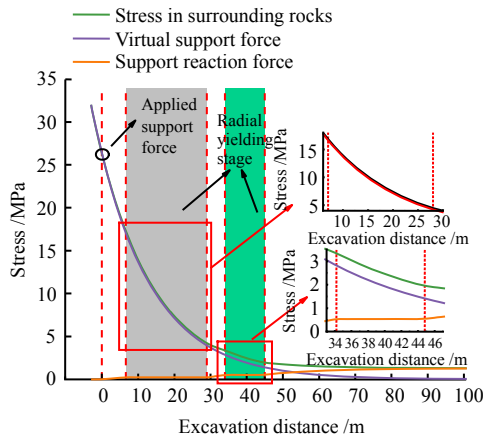

Fig. 7 Variation of stress with excavation distance

$$k^* = \frac{p^*}{p^*_{\text{in}}} \tag{46}$$

where p^* is the virtual support force and p^*_{in} is the virtual support force in the initial state.

Based on the convergence constraint method, the initial virtual support force p^*_{in} is obtained by extracting the stress around the excavation surface under the equilibrium condition. $x=-\infty$ is substituted into the Vlachopoulos formula to obtain the virtual support force when the distance between the excavation surface and the studied section is infinite, that is, the initial virtual support force is

$$p^*_{\text{in}} = p_\infty \tag{47}$$

The virtual support force during the excavation can be obtained by the Vlachopoulos formula, and the corresponding virtual support force release rate can be obtained by substituting it into Eq. (46):

$$\left.\begin{aligned} k^*(x) &= \left(1-\delta_0^*\right)\exp\left(x^*\right) \quad \left(x^*<0\right)\\ k^*(x) &= \left(1-\delta_0^*\right)\exp\left(-\frac{3x^*}{2r^*}\right) \quad \left(x^*\geqslant 0\right)\\ \delta_0^* &= \frac{1}{3}\exp\left(-0.15r^*\right) \end{aligned}\right\} \tag{48}$$

By defining the excavation speed of the numerical simulation, both the relationship between the release rate of the virtual support force and the time and the amplitude curve of the virtual support force release rate can be obtained. Assuming that the excavation speed is v, the relationship between the release rate of the virtual support force and the time can be obtained by substituting $x=vt$ into Eq. (48):

$$\left.\begin{aligned} k^*(t) &= \left(1-\delta_0^*\right)\exp\left(t^*\right) \quad \left(t^*<0\right)\\ k^*(t) &= \left(1-\delta_0^*\right)\exp\left(-\frac{3t^*}{2r^*}\right) \quad \left(t^*\geqslant 0\right)\\ \delta_0^* &= \frac{1}{3}\exp\left(-0.15r^*\right) \end{aligned}\right\} \tag{49}$$

where $t^* = \dfrac{vt}{r_0}$ and t is the advance time of the excavation surface. $t>0$ indicates that the studied section is located behind the excavation surface. $t<0$ indicates that the studied section is located in front of the excavation surface.

In this paper, the excavation speed is set to 2 m/d in the numerical simulation, and the amplitude curve of the virtual support force release rate can be calculated.

7.2 Implementation of yielding stage

According to the characteristics of the graded yielding support structure, the arch frame is equivalent to the solid element with a certain thickness in order to simulate the two yielding stages and control the yielding amount, and it is divided into the outer arch frame deformation layer, the transition layer 1, the inner arch frame deformation layer, the transition layer 2, and the support layer from outside to inside. The yielding layer is reserved for the deformation layer of the inner and outer arch frames. The material properties of the yielding layer and the transition layer are consistent with those of the support layer at the strong support stage. At the yielding stage, the material properties are converted to the yielding parameters. The sign of entering the yielding stage is that the internal force of the support structure reaches the yielding point, and the internal force of the structure is increasing under the combined effect of the stress in the surrounding rocks and the virtual support force. The analysis step of the yielding stage is determined by the amplitude curve of the virtual support force, and the elastic modulus and the Poisson's ratio of the material are modified in the model file 'Keywords' to achieve the yielding effect.

7.3 Model establishment

In order to verify the reliability of the yielding support under the high-stress setting, a two-dimensional model with a size of 100 m×100 m was established based on the geological characteristics of the Shawan Tunnel, and the excavation radius of the tunnel is 5.5 m and the initial stress is 32 MPa. The Mohr-Coulomb model and the elastic model were used to simulate the surrounding rocks and the support structure, respectively. The yielding point is 0.5 MPa for the support structure, and the two yielding amounts of the arch frame are 0.08 m and 0.05 m, respectively. The mechanical parameters of the surrounding rocks and the support structure are shown in Table 3.

Table 3 Main parameters of tunnel surrounding rocks and support structure

Materials	Elastic modulus E/GPa	Poisson's ratio v	Cohesion c /MPa	Internal friction angle φ/(°)
Surrounding rocks	0.2	0.35	2.0	30
Support structure	210	0.25		

According to the literature [28], the elastic modulus of the steel frame is equivalent to the elastic modulus of a solid element:

$$E_{\text{s}} = \frac{S_{\text{g}}E_{\text{g}}}{S_{\text{S}}} \tag{49}$$

where S_{g} is the cross-section area of the steel frame; E_{g} is the elastic modulus of the steel frame; and S_{S} is the cross-section area of the solid element.

The equivalent elastic modulus of the solid element is 100 GPa, and the elastic modulus of the solid element at the yielding stage is equivalent to 3 MPa. From the spatial effect of the excavation surface, it can be seen that the stress in the surrounding rocks has been partially released before the tunnel is excavated. At the same time, the release of the stress in the surrounding rocks in advance is also considered in the theoretical analysis. In order to verify the rationality, the stress in the surrounding rocks after the excavation is taken as the outer boundary force at the initial strong support stage in the theoretical analysis. Through Eq. (1), the initial stress in the surrounding rocks in the theoretical analysis can be calculated as 34 MPa.

The whole calculation process is divided into 7 stages: (1) geostress balance; (2) excavation and support; (3) first strong support stage; (4) radial yielding stage; (5) secondary strong support stage; (6) circumferential yielding stage; (7) subsequent strong support stage.

7.4 Comparative verification of calculation results

Figure 8 gives the comparative curves of the calculated and simulated vertical stresses in the surrounding rocks at the vault. The results show that the change trends of these two curves are the same, and the stresses of both are obviously released at the yielding stage. Under the influence of the spatial effect of the excavation surface, the support reaction force increases rapidly at the early stage of the support, so that the support structure enters the radial yielding stage. The stress in the surrounding rocks is significantly released at this stage. At the later stage of the deformation of the surrounding rocks, the virtual support force is small, and the surrounding rocks remain stable under the action of the support structure. The release law of the stress in the surrounding rocks shows that the deformation of the support structure should conform to the stress release characteristics of the surrounding rocks, the higher yielding deformation is provided at the early stage of the support, and the strong deformation resistance ability is provided at the later stage of the support.

7.5 Analysis of numerical simulation results

7.5.1 Displacement variation of surrounding rocks

Figure 9 presents the vertical displacement cloud diagram of the surrounding rocks. Under the pressure of the surrounding rocks, significant deformation occurs at the vault and the arch floor. The sinking of the vault is about 12 cm, and the heaving of the arch floor is about 16 cm.

The deformation of the vault and the arch floor at the first strong support stage is 1.7 cm and 1.5 cm, respectively. The support strength at this stage is high, and the support reaction force provided by the support structure increases rapidly. The yielding deformation with constant resistance is produced in the support structure at the radial yielding stage. The deformation of the surrounding rocks increases accordingly, and the deformation of the vault and the arch floor is 7.5 cm and 8.8 cm respectively at this stage. At the secondary strong support stage, the support structure slows down the deformation of the surrounding rocks, and a slight deformation is produced in the surrounding rocks under the strong support of the support structure. The shrinkage deformation is further produced in the support structure at the circumferential yielding stage, and the deformation of the surrounding rocks at the vault and the arch floor is 4.3 cm and 2.8 cm. After the yielding deformation of the support structure, only the elastic deformation is produced in the structure, so that only minor deformation is produced in the surrounding rocks at this stage. In summary, the deformation of the surrounding rocks mainly occurs at the yielding stage of the structures. The deformation generated at the yielding stage accounts for about 80% of the total deformation, which greatly reduces the elastic deformation of the support structure, thereby reducing the internal force of the structure and ensuring the stability of the support structure.

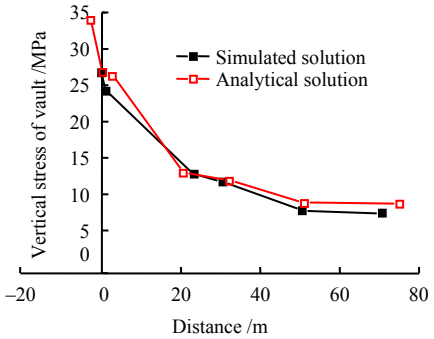

Fig. 8 Comparison of simulated vertical surrounding rock stress of vault with that of the analytical solution

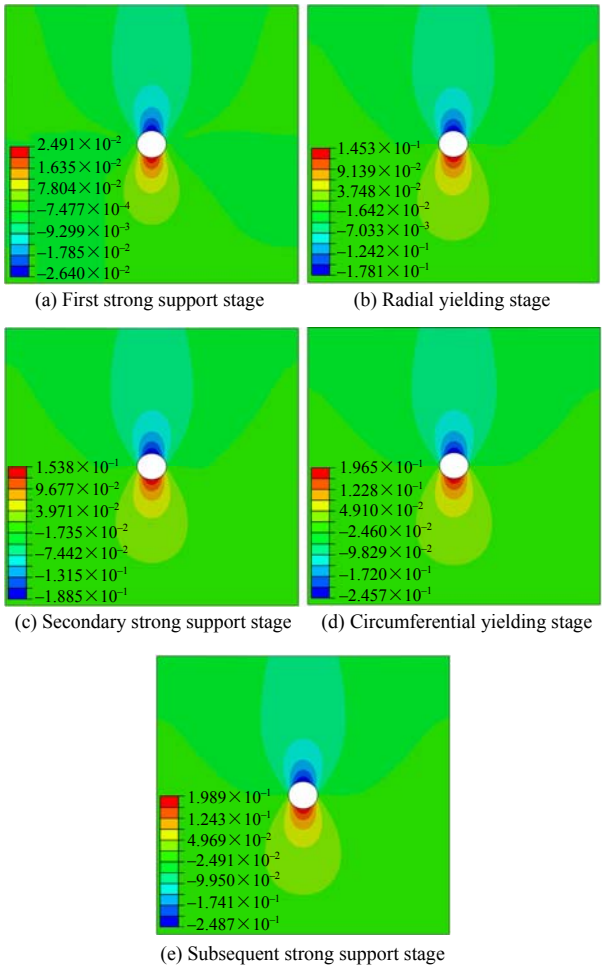

(a) First strong support stage (b) Radial yielding stage

(c) Secondary strong support stage (d) Circumferential yielding stage

(e) Subsequent strong support stage

Fig.9 Evolution of vertical displacement in surrounding rocks (unit: m)

Figure 10 illustrates the variation of the vertical displacement of the surrounding rocks. The results show that the displacement around the tunnel is symmetrically distributed. The vertical displacement of the surrounding rocks mainly occurs at the vault and the arch floor, and it significantly increases during the yielding stage. The stress in the surrounding rocks is high at the radial yielding stage and the stress release is significant, so that the stress in the structure quickly reaches the yielding point and the yielding deformation is produced. At the circumferential yielding stage, the stress in the surrounding rocks is significantly released, and its impact on the structure deformation is small. Therefore, the yielding amount of the structure at the radial yielding stage can be appropriately provided to suit the stress release characteristics of the surrounding rocks and ensure the stability of the support structure.

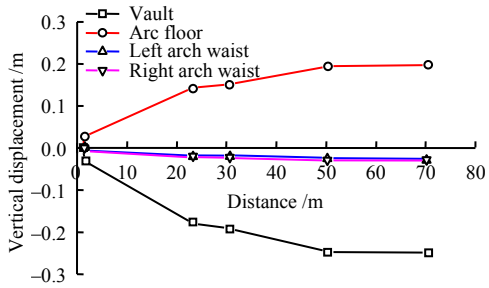

Fig. 10 Displacement curves

7.5.2 Variation of stresses in surrounding rocks

Figure 11 shows the cloud map of the vertical stress variation in the surrounding rocks. The deformation of the surrounding rocks is smaller at the first strong support stage, resulting in lower stress release, and the stress peak occurs at the vault and the arch floor. When the deformation of the surrounding rocks enters the radial yielding stage, the deformation at the vault and the arch floor is great, causing a significant release in the stress and the shift of the peak stress location to both sides of the arch waist. At the same time, stress concentrations occur in the surrounding rocks at both sides of the arch waist due to vertical compression, resulting in an increase in the stress in the surrounding rocks at both sides of the arch waist. Subsequently, at the secondary strong support stage and the circumferential yielding stage, the stress release of the surrounding rocks occurs at the vault and the arch floor, but there is a stress increase at both sides of the arch waist. The support structure maintains the stability of the surrounding rocks at the later strong support stage, so that the stress release in the surrounding rocks is less at the vault and the arch floor, and the stress growth at both sides of the arch waist is slowed down. In summary, the yielding support releases the vertical stress in the surrounding rocks at the vault and the arch floor, and also increases the stress at both sides of the arch waist.

Figure 12 shows the variation of the vertical stress in the surrounding rocks. Vertical stresses of the surrounding rocks are released at the vault and the arch floor and are mainly concentrated at the two yielding stages. The stress growth occurs at both sides of the arch waist, especially at the radial yielding stage, which is consistent with the cloud map shown in Fig. 11.

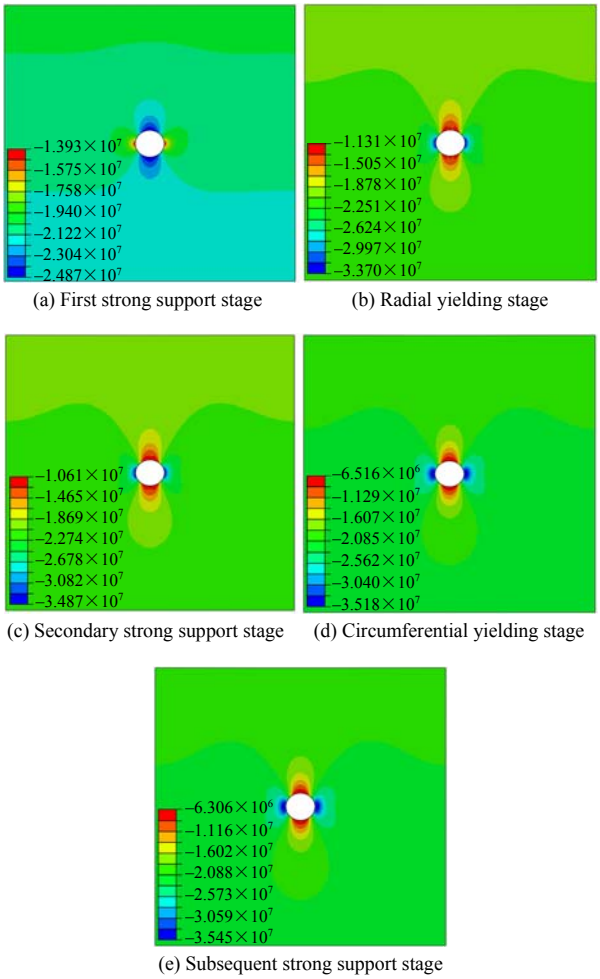

Fig. 11 Evolution of vertical stress in surrounding rocks

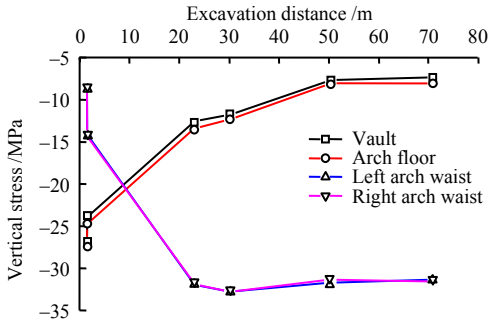

Fig. 12 Variation of stresses in surrounding rocks

8 Conclusions

(1) According to the deformation characteristics of the tunnel in the soft rock under high geostress, a new graded yielding support structure is proposed. The support structure can achieve the effect of increasing the yielding amount through the two yielding levels at the inner and outer arch frames. Based on the deformation characteristics of the support structure, the deformation of the support structure is divided into the first strong support stage, the radial yielding stage, the secondary strong support stage, the circumferential yielding stage, and the subsequent strong support stage.

(2) Based on the spatial effect of the excavation surface and the characteristics of different deformation stages of the yielding structure, the virtual support force

and the strain softening conditions of the surrounding rocks are introduced, and the static equilibrium equation of the stress in the surrounding rocks, the virtual support force, and the support reaction force is established, which reveals the deformation and stress release law of the surrounding rocks at each stage.

(3) The stress release law of the surrounding rocks is consistent with the growth law of the support reaction force, and both of them have significant stages. The stress in the surrounding rocks is significantly released during the yielding stage, while the support reaction force significantly increases during the strong support stage.

(4) The distribution laws of the theoretical calculation and numerical simulation results are the same. The proposed support structure can effectively release the stress in the surrounding rocks, reduce the structure force, and effectively avoid the failure of the support structure due to excessive loading.

References

[1] JIANG Yun, LI Yong-lin, LI Tian-bin, et al. Study of the classified system of types and mechanism of great distortion in tunnel and underground engineering[J]. Journal of Geological Hazards and Environment Preservation, 2004, 15(4): 46–51.

[2] DING Yuan-zhen, TAN Zhong-sheng, MA Dong. Study on large deformation characteristics and control measures of soft rock tunnel in fault zone with high geostress[J]. China Civil Engineering Journal, 2017, 50(Suppl.1): 129–134.

[3] LI Lei. Study on squeezing large deformation mechanism and control technology of phyllite tunnel[D]. Beijing: Beijing Jiaotong University, 2017.

[4] GUO Xiao-long, TAN Zhong-sheng, LI Lei, et al. Deformation and failure mechanism of layered soft rock tunnel under high stress[J]. China Civil Engineering Journal, 2017, 50(Suppl.2): 38–44.

[5] CAO Xiao-ping, WEI Fei-peng, WANG Bo, et al. Experimental study on reasonable support scheme for high ground stress soft rock tunnel[J]. Journal of Railway Engineering Society, 2018, 35(7): 65–71, 102.

[6] MA Zhao-lin, JIAO Lei, ZHAO Shuang, et al. Safety analysis of re-applied section of high ground stress soft rock tunnel lining[J]. Tunnel Construction, 2018, 38(9): 1489–1496.

[7] KIMURA FUMINORI, OKABAYASHI NOBUYUKI, KAWAMOTO TOSHIKAZU. Tunnelling through squeezing rock in two large fault zones of the Enasan Tunnel II[J]. Rock Mechanics and Rock Engineering, 1987, 20(3): 151–166.

[8] GANTIENI L, ANAGNOSTON G. The interaction between yielding supports and squeezing ground[J]. Tunnel and Underground Space Technology, 2009, 24(3): 309–322.

[9] ANAGNOSTON G, GANTIENI L. Design and analysis of yielding supports in squeezing ground[C]//Proceedings of 11th ISRM Congress. Lisbon: [s. n.], 2007, 9–13.

[10] KOVÁRI K, AMSTAD C, ANAGNOSTOU G. Design/ construction methods: tunnelling in swelling rocks[C]// The 29th US Symposium on Rock Mechanics (USRMS). [S. l.]: American Rock Mechanics Association, 1988.

[11] HE Man-chao, GUO Zhi-biao. Mechanical property and engineering application of anchor bolt with constant resistance and large deformation[J]. Chinese Journal of Rock Mechanics and Engineering, 2014, 33(7): 1297–1308.

[12] QIU Wen-ge, WANG Gang, GONG Lun, et al. Research and application of resistance-limiting and energy-dissipating support in large deformation tunnel[J]. Chinese Journal of Rock Mechanics and Engineering, 2018, 37(8): 1785–1795.

[13] WANG Bo, WANG Jie, WU De-xing, et al. Discussion on application of yielding supporting technology in large-deformation tunnel in soft rock[J]. Journal of Highway and Transportation Research and Development, 2015, 32(5): 115–122.

[14] WANG Bo, WANG Jie, WU De-xing, et al. Study on application of yielding supporting system for large-deformation in soft rock highway tunnel[J]. Journal of Railway Science and Engineering, 2016, 13(10): 1985–1993.

[15] WEN Jing-zhou, YANG Chun-lei, SU Hai-tao, et al. Theoretical analysis and application of composite arch for bolt-shot concrete steel frame supported tunnel in weak and fractured rock mass[J]. China Civil Engineering Journal, 2015, 48(5): 115–122.

[16] CUI Lan. Interaction between support and surrounding rock considering strain-softening behaviour for deep tunnelling[D]. Wuhan: Huazhong University of Science and Technology, 2016.

[17] HOU Gong-yu. Interaction mechanism of surrounding rock-support based on the spatial effect of excavating face[J]. Chinese Journal of Rock Mechanics and Engineering, 2011, 30(Suppl.1): 2871–2877.

[18] HOU Gong-yu, LI Jing-jing. Analysis of complete process of interaction of surrounding rock and support under elastoplastic deformation condition[J]. Rock and Soil Mechanics, 2012, 33(4): 961–970.

[19] FU Guo-bin. Recent investigation of extent of fractured zone and displacement of rocks around the roadways[J]. Journal of China Coal Society, 1995, 20(3): 304–310.

[20] WANG Hua-ning, LI Yue, LUO Li-sha, et al. Analytical research of mechanical response of TBM construction in strain-softening elasto-plastic rock[J]. Chinese Journal of Rock Mechanics and Engineering, 2016, 35(2): 356–368.

[21] SUN Zhen-yu, ZHANG Ding-li, FANG Qian, et al. Spatial and temporal evolution characteristics of interaction between primary support and tunnel surrounding rock[J]. Chinese Journal of Rock Mechanics and Engineering, 2017, 36(Suppl.2): 3943–3956.

[22] VLACHOPOULOS N, DIEDERICHS M S. Improved longitudinal displacement profiles for convergence confinement analysis of deep tunnels[J]. Rock Mechanics and Rock Engineering, 2009, 42(2): 131–146.

[23] ALEJANO L R, RODRIGUEZ-DONO A, VEIGA M. Plastic radii and longitudinal deformation profiles of tunnels excavated in strain-softening rock masses[J]. Tunnelling and Underground Space Technology, 2012, 30(1): 169–182.

[24] CARRANZA-TORRES C, FAIRHURST C. Application of the convergence-confinement method of tunnel design to rock masses that satisfy the Hoek-Brown failure criterion[J]. Tunnelling and Underground Space Technology, 2000, 15(2): 187–213.

[25] CARRANZA-TORRES C, FAIRHURST C. The elasto-plastic response of underground excavations in rock masses that satisfy the Hoek-Brown failure criterion[J]. International Journal of Rock Mechanics and Mining Sciences, 1999, 36(6): 777–809.

[26] ZHENG Yu-tian. Fundamentals of elasticity, plasticity, and viscosity theory of rock mechanics[M]. Beijing: China Coal Industry Press, 1988.

[27] GUAN Bao-shu. General theory of tunnel mechanics[M]. Chengdu: Southwest Jiaotong University Press, 1993.

[28] LI Shu-cai, WANG Shu-fa, ZHU Wei-shen, et al. Research on numerical simulation of deformation of soft rockmass tunnels in Taiwan[J]. Chinese Journal of Geotechnical Engineering, 2001, 23(5): 540–543.